Resource Assessment of Ocean Thermal Energy Conversion in Puerto Rico

Fadia Ticona Rollano[a], Gabriel García Medina[b], Zhaoqing Yang[a,c,*], Andrea Copping[a,d]

[a] *Coastal Sciences Division, Pacific Northwest National Laboratory, Seattle, 98109, WA, USA*
[b] *Mott MacDonald, Seattle, 98101, WA, USA*
[c] *Department of Civil and Environmental Engineering, University of Washington, Seattle, 98195, WA, USA*
[d] *School of Marine and Environmental Affairs, University of Washington, Seattle, 98195, WA, USA*

Abstract

Island communities often struggle to establish traditional electric grids and are heavily reliant on imported fossil fuels. For Puerto Rico (PR), these challenges are enhanced by extreme weather and other natural hazards that threaten the local electric infrastructure. Ocean thermal energy conversion (OTEC) could play an important role in establishing a more resilient electrical grid in the region. A detailed analysis is conducted to characterize the ocean thermal resource and power potential of OTEC in PR based on a 14-year dataset of modeled ocean temperature. The assessment considers seasonal and interannual thermal patterns, examining the operational limitations associated with running a typical OTEC plant. The local thermal resource is found to be sensitive to El Niño-Southern Oscillation climate patterns, with La Niña conditions linked to greater OTEC power availability. Six areas of opportunity are identified based on their resource potential and proximity to existing electrical transmission lines, including one that could

*Corresponding author email: zhaoqing.yang@pnnl.gov.

also benefit the nearby U.S. Virgin Islands. The greatest OTEC power potential is observed to the south of PR with an estimated capacity of 138 MW for a plant pumping cold water from a depth of 1,000 m, or the equivalent amount of electricity required to power 219,000 households.

Keywords: ocean thermal energy, OTEC, Puerto Rico, energy resilience, resource characterization, U.S. Virgin Islands

1. Introduction

The Commonwealth of Puerto Rico (henceforth PR) enacted a public policy to generate 100% of its electricity from renewable sources by 2050 in an effort to increase its resilience to extreme weather and reduce its reliance on fossil fuels [1]. This commitment follows a long track record of power outages driven by recurring natural hazards, including hurricanes and earthquakes, in addition to an unreliable electrical system that is largely overdue for upgrades and repairs [2]. The power demand in PR frequently surpasses the electricity that can be generated and distributed through the current grid, even during off-peak conditions, leading to a dependence on imported fuels [3]. According to the U.S. Energy Information Administration, PR consumes about 70 times more energy than it produces and, in 2022, 94% of its electricity was generated from fossil fuels [4]. Ocean thermal energy conversion (OTEC) could play a significant role in PR's energy transition, providing a fairly consistent source of electricity and diversifying the local energy portfolio [5].

OTEC is a process used to generate power from the difference in temperature between cold deep-sea water and warm, sun-heated, surface seawater

[6]. The notion of this technology was first proposed by the French physicist Jacques-Arsene D'Arsonval in 1881 [7]. The most common design for an OTEC system is based on the thermodynamic principles of a Rankine cycle heat engine. The OTEC Rankine cycle consists on leveraging phase changes of a working fluid, driven by controlled heat exchanges with seawater, to convert thermal energy into mechanical energy. More specifically, the working fluid (e.g., ammonia) recirculates in a closed loop and interacts with four main components: an evaporator, a condenser, a turbine, and a pump [8]. At the evaporator, heat from the surface seawater is transferred to the working fluid via heat exchangers resulting in a phase change from liquid to gas. Next, the working fluid vapor activates a turbine to convert the thermal energy into mechanical energy–which can in turn be used to produce electricity using a generator. From there the working fluid vapor goes back to its liquid state at the condenser, where additional heat exchangers transfer its heat to cold deep-sea water. The cycle is completed by sending the working fluid back up to the evaporator through the pump. Because of its characteristic closed loop for the working fluid, this type of scheme is also referred to as *closed-cycle* OTEC. In contrast, *open-cycle* OTEC, uses the intake seawater as the working fluid in a different type of heat engine cycle, generating freshwater as a bi-product of electricity. While in all likelihood the added benefit of generating freshwater may be of interest to certain communities in PR, this study is limited to thermal energy conversion for the sole purpose of generating electricity. Similarly, there are several other types of OTEC cycles encountered in the literature, but the Rankine cycle is by far the most regularly used in resource assessments, and is the chosen cycle

for the present study. A more detailed review of OTEC technology can be found in [9] and more recently in [10].

An inherent challenge with OTEC is the low energy conversion efficiency that results from the low temperature differentials between surface and deep seawater as compared to traditional large-scale heat engines. The minimum temperature differential required for OTEC operation is 20^oC, corresponding to a conversion efficiency of 3-4% [11, 9, 12]. According to [13], an increase of 2^oC above this threshold could lead to an efficiency increase of over 20%. Consequently, siting OTEC at locations with relatively strong ocean thermal gradients is critical for optimal operation. Additionally, the closer the thermal resource is to shore, the more affordable it is to transfer the energy harvested at an OTEC plant to an onshore electrical grid [14]. Considering both of these factors, OTEC is particularly suitable for coastal regions in the tropics and subtropics, where the thermal gradients are strong thanks to warmer-than-average surface temperatures, and where the deep ocean is accessible close to shore because of the steep slopes characteristic of volcanic topography.

OTEC technology was demonstrated in 1979 during a pilot scale experiment conducted at the Natural Energy Laboratory of the Hawaiian Authority (NELHA), which generated over 50 kW of gross power and 18 kW of net power [15]. Soon after, in 1981, a consortium of Japanese companies led by Tokyo Electric Power commissioned a demonstration-scale OTEC plant on the island of Nauru that produced 120 kW of gross power and 30 kW of net power [16]. Despite the success of these early experiments, and additional demonstration-type projects in more recent years [17, 18, 19] with

a maximum achieved power rating of 338 kW [20], there have not been any commercial-scale developments of OTEC to date. This can be largely explained by the relatively large capital costs required to establish an OTEC plant [7, 21, 22] yet techno-economic studies suggest that the cost-to-benefit ratio would improve for OTEC plants of a sufficiently large power capacity (of least 10 MW [23] but ideally 50–100 MW). Numerical models can play an important role in ushering the OTEC industry towards commercialization by providing a high-fidelity characterization of ocean thermal resources that can be used to site OTEC plants in optimal locations across the world thus reducing the risk of capital investment.

Models for estimating the power potential of OTEC have improved from early one-dimensional studies [11, 24] to much more accurate three-dimensional ocean circulation models [12, 25] which predict that the global OTEC power potential could reach up to 10 TW. Additionally, one study predicts that the OTEC power potential could increase by 46% by the end of the century assuming a global greenhouse warming scenario with high carbon emissions [26]. More detailed resource assessments are conducted at regional scales using higher resolution models [27, 28, 29, 30, 17, 31].

A plan for a conceptual 40 MW pilot OTEC plant at Punta Tuna, PR, was released in 1981 [32, 33], but the initiative did not advance beyond engineering design. The potential for OTEC in PR was explored more generally as part of a global assessment of the thermal energy resource in a report prepared by Lockheed Martin with the sponsorship of the U.S. Department of Energy (DOE) [5]. The study was based on a proprietary OTEC plant design and a 2-year data record of ocean temperature obtained from the HYbrid

Coordinate Ocean Model (HYCOM). The results of the assessment quantified the thermal energy resource for OTEC in the regions of top interest in the U.S. exclusive economic zone (EEZ)—including the U.S. Caribbean Sea and Pacific islands, the East Coast and the Gulf of Mexico—and in United Nations Recognized EEZs. The top highlighted regions in the U.S. include Hawaii, the Mariana Islands, Guam, PR, and the U.S. Virgin Islands (henceforth USVI). The combined annual technical resource potential for OTEC in PR and the USVI was of 38 TWh, assuming the use of Lockheed Martin's technology. The results of this assessment were reviewed in two subsequent reports–also sponsored by the U.S. DOE–in the context of marine renewable energy potential in the U.S. EEZ [34, 35]. Both reports indicated the need for further analysis of the thermal resource that should include a substantially longer data record and that would ideally be independent of any specific OTEC plant designs so the results could instead be used for the analysis of varying technologies, but concurred on the general location of the highlighted regions with highest OTEC potential.

Although previous studies have included PR and USVI in their analyses, our study is the first detailed characterization of the OTEC potential in the region based on high resolution data over an extended period of time (14 years). This work aims to describe the spatial and temporal patterns of the OTEC thermal resource based on a technology agnostic approach that could be adapted to the particular characteristics of a broad range of Rankine-cycle OTEC plant designs. The analysis quantifies the annual energy production at six areas of opportunity for potential OTEC installations, incorporating operation technological factors that may cause the plants to pause their power

production. Further, while other physical processes such as rainfall and wind patterns have been studied with relation to ENSO climate patterns in the region, these effects have not been studied in the context of OTEC power production. We anticipate that the characterization of such trends will have a direct impact on the design and operation considerations of future OTEC plants in terms of power efficiency optimization.

This study presents a focused resource assessment of thermal energy potential for the implementation of OTEC technology in PR based on 14 years of ocean hindcast data. Section 2 describes the ocean model dataset obtained to characterize the thermal resource in the region. The model performance is evaluated through a statistical error analysis against in-situ observations (from profiling floats and satellites). The methodology used to calculate the OTEC power density is also provided in Section 2. Section 3 presents seasonal and annual geographic distributions of power density relative to cold water inflow and considers the influence of picking different depths of cold water intake. Section 4 expands on the discussion of the OTEC operational limitations relative to the thermal gradient between the surface and deep water through a time series analysis of select areas of opportunity in the region, including PR coastal waters as well as nearby USVI. Conclusions are presented in Section 5.

2. Methods

2.1. Model selection and data acquisition

The ocean thermal gradients around PR and the USVI are analyzed based on a 14-year record of three-dimensional (3D) sea temperature obtained from

the global ocean circulation model HYbrid Coordinate Ocean Model (HYCOM) [36]. This is the same model that was used in the aforementioned OTEC assessment by Lockeed Martin [5], however, that study was based on only 2 years of data, which is not sufficient to accurately assess the long-term resource and the seasonal variability. The 14-year HYCOM dataset was the longest available record of 3D ocean temperatures within the study area at the time of data collection. Opting for a longer time record allows for an evaluating of seasonal reoccurring trends as well as the influence of low frequency climate patterns such as El Niño-Southern Oscillation (ENSO) cycles.

The HYCOM results considered in this study correspond to two implementations of the model, Global Ocean Forecasting System (GOFS) 3.0 and GOFS 3.1. The two GOFS versions overlap from July 2014 to November 2018. A comparison of the overlapping record lengths showed little variability ($< 0.5^{o}$C) in monthly (not shown) and annual (Figure 1) averages of sea surface temperature within the PR and USVI EEZ. For the purpose of this study, the HYCOM records were combined using GOFS 3.0 from September 2008 through June 2014 and GOFS 3.1 as of July 2014 through December 2021. A summary of both GOFS implementation is shown in Table 1. The vertical resolution of HYCOM (33 to 44 layers) is well suited for resolving the thermocline and mid water-column temperature gradients. HYCOM's computational grid, with a horizontal resolution of about 9 km and 5,872 nodes within the PR/USVI EEZ, provides a good basis for characterizing the spatial variability of the thermal resource at a regional scale.

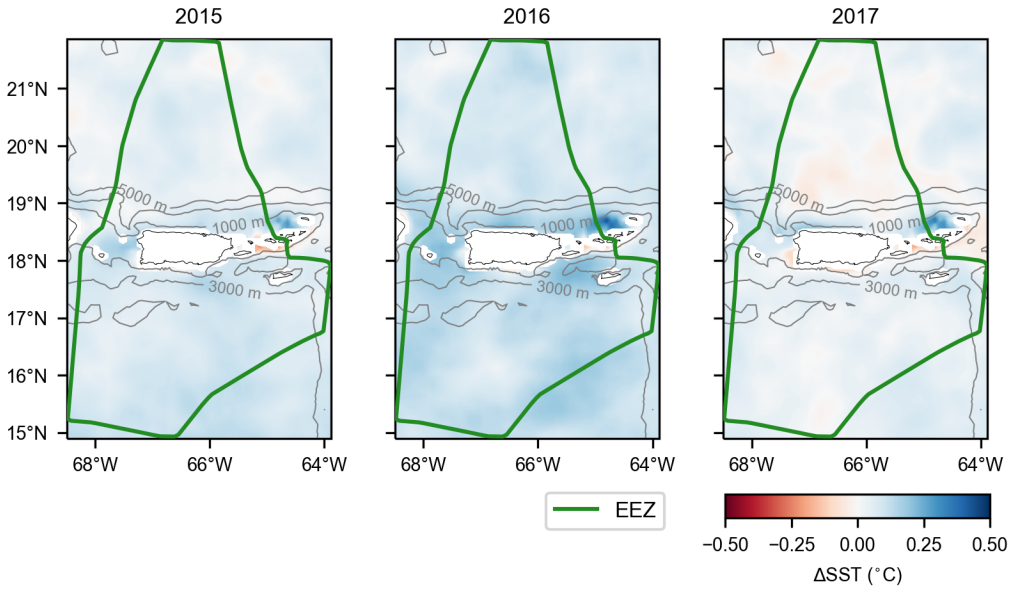

Figure 1: Average difference in temperature between HYCOM GOFS versions 3.0 and 3.1 during complete overlapping years.

Table 1: HYCOM GOFS model properties

Properties	**Version 3.0**	**Version 3.1**
Record length	2008 – 2018	2014 – 2021
Horizontal resolution	$1/12^o$	$1/12^o$
Horizontal resolution in meridional direction (km)	9.2	9.2
Horizontal resolution in zonal direction at 18^oN (km)	8.8	8.8
Number of vertical levels	33	40
Vertical layer depth (m)	0, 10, 20, 30, 50, 75, 100, 125, 150, 200, 250, 300, 400, 500, 600, 700, 800, 900, 1000, 1100, 1200, 1300, 1400, 1500, 1750, 2000, 2500, 3000, 3500, 4000, 4500, 5000, 5500	0, 2, 4, 6, 8, 10, 12, 15, 20, 25, 30, 35, 40, 45, 50, 60, 70, 80, 90, 100, 125, 150, 200, 250, 300, 350, 400, 500, 600, 700, 800, 900, 1000, 1250, 1500, 2000, 2500, 3000, 4000, 5000

HYCOM is independently calibrated but for use in this study we compare the collected dataset against historical records to verify its accuracy. Sea surface temperature (SST) from the combined HYCOM data record is compared to satellite imagery from the Multi-scale Ultra-high Resolution (MUR) SST analysis (Figure 2). HYCOM's average seasonal predictions of SST are lower than the satellite measurements by no more than $< 0.5^{o}$C, with greater variability shown within coastal regions which, in any case, is in depths too shallow for OTEC considerations. HYCOM thermal profiles are verified against ARGO float measurements with 99% of the modeled data falling within a $< 1.5^{o}$C range from the measurement (Figure 3).

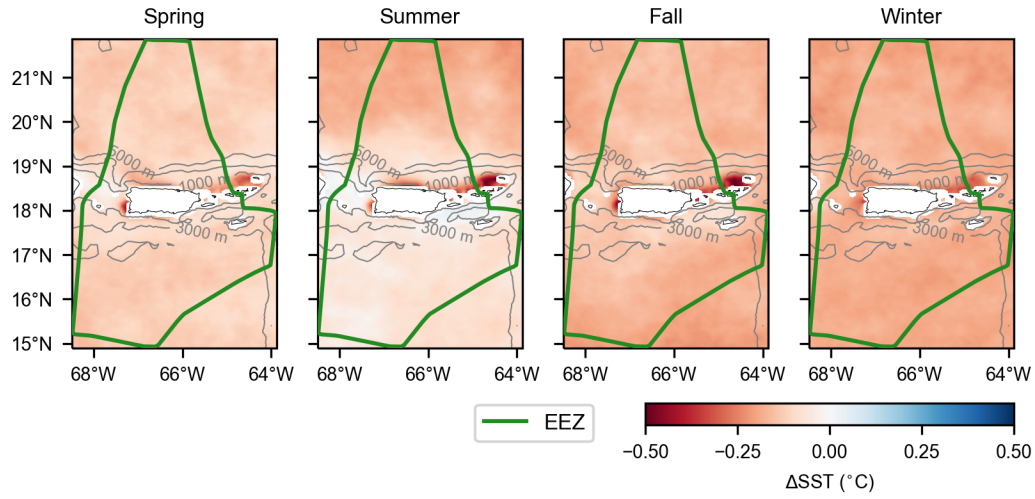

Figure 2: Seasonal difference in mean SST between HYCOM and MUR for 2008—2021. Warm colors indicate satellite measurements are higher (i.e., hotter) than model predictions.

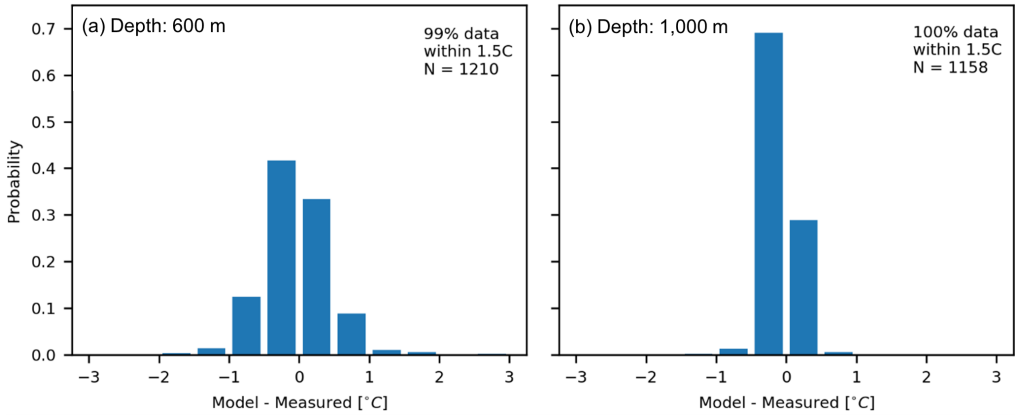

Figure 3: Average difference in temperature between HYCOM and Argo floats at (**a**) 600 m and (**b**) 1000 m water depth.

2.2. Estimation of power density

The power density for OTEC systems is expressed as the net power P_{net} per unit of upwelled cold water flowrate Q_{CW} and estimated as

$$\frac{P_{net}}{Q_{CW}} = \frac{\rho_w C_p E_{TG} (\Delta T)^2 (1 - PL)}{8(273 + T_s)} \tag{1}$$

where:

- ρ_w is the average density of water, taken as 1,024 kg/m^3,
- C_p is the specific heat of water, taken as 4.184 J/g^{o}C,
- E_{TG} is the turbogenerator efficiency,
- ΔT is the net difference between the warm water intake temperature near the surface and the cold water intake temperature,
- PL is the pumping loss of energy as a function of pipe length, and
- T_s is the near the surface intake temperature.

Equation 1 is an adaptation of [11] as seen in [5, 34] based on the assumption that the small temperature range in the ocean results in negligible nonlinear effects. To ensure this assumption holds, it is important to consider a warm water intake depth deeper than the true ocean surface which can be prone to significantly more temperature variability. Placing the warm water intake pipe below the surface also keeps it from being exposed to the elements and prevents inconsistent intake flows. The depth of the warm water intake may vary with plant designs, with typical values between 20 m [5, 7, 9] and 75 m [11]. In this study, T_s corresponds to the 50 m depth layer from the HYCOM dataset. The turbogenerator efficiency and energy loss terms are also dependant upon the design of the OTEC system. In this study, we set

E_{TG} as 1 and PL as 0, to conduct a technology agnostic analysis (i.e., the turbogenerator is assumed to be 100% efficient and the system is assumed to have no energy losses due to pumping). In this way, the power that a specific OTEC plant would produce could be obtained by multiplying the results presented in this study by its own efficiency and energy loss factor (that is, multiplying the power results from this study by $E_{TG} \times (1 - PL)$ characteristic of a specific plant).

The expected influence of the error in HYCOM temperature predictions, as compared to MUR and Argo measurements, and applied to the OTEC power calculation is considered in Figure 4. The difference in power estimate is obtained by isolating the temperature terms in Equation 1, that is $\frac{(\Delta T)^2}{(273+T_s)}$, and conducting a simple sensitivity analysis based on the temperature differences observed in Figures 2 and 3 and sample benchmark temperatures at a location to the south of mainland PR (corresponding to cluster S1 presented later in Figure 11). Based on this analysis, the model underpredictions of SST in the order of 0.5^oC would result in a 4.4% underprediction of OTEC power.

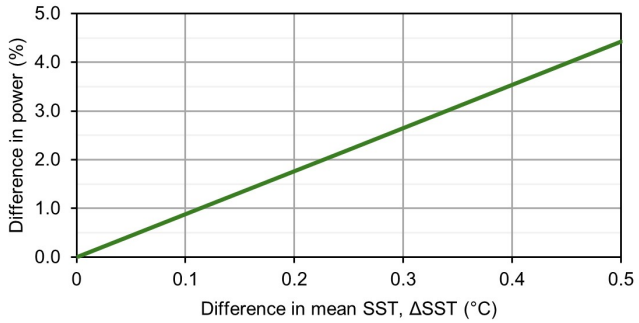

Figure 4: Influence of error in HYCOM temperature predictions in power estimates.

The net power, or OTEC plant capacity, is obtained from the product of the power density multiplied by the upwelled cold water flowrate. The annual energy production (AEP) can then be calculated as the net power times the total hours in a year (or 8,760).

3. Results

3.1. Characterization of the ocean thermal resource

The 14 year HYCOM data record was used to compute average distributions of the surface temperature, T_s, and the thermal gradients, ΔT, around PR and the USVI. The seasonal distributions of T_s–taken at a 50 m depth– and ΔT–calculated between the surface and a sample depth of 1,000 m–are shown in Figures 5 and 6, respectively. The warmest surface temperatures and highest thermal gradients are observed in the spring (March 1 to May 31), while the coldest temperatures and lowest thermal gradients are observed in the fall (September 1 to November 30). Surface temperature tends to be greater in the Caribbean Sea as compared to the Atlantic Ocean and this trend becomes more evident with greater distance away from the PR coast. These relative trends carry down the water column resulting in a more pronounced ΔT variation between north and south by up to 1^oC.

Time series provide deeper insights into the seasonal variability of the ocean thermal resource. Figure 7 shows time series of T_s and ΔT for a sample location to the south of mainland PR (corresponding to cluster S1 presented later in Figure 11). The sea surface temperature peaks annually between September and October when T_s is about 29^oC. The coldest surface temperatures are observed in February and March when T_s can go below

26^{o}C.

The OTEC ocean thermal resource in PR and the USVI is influenced by climate variability arising from meteorological events such as tropical storms and hurricanes, as well as interannual anomalies such as El Niño–Southern Oscillation (ENSO). In the PR and USVI region, the effects of ENSO are different in the dry season (December to April) than in the wet season (May to November). In the dry season, El Niño years are associated with increased precipitation and cooler SST, while La Niña years are associated with close to neutral or slightly lower precipitation. Conversely, in the wet season, El Niño years are associated with reduced precipitation, leading to drought and a reduction of the number of tropical storms, while La Niña years are associated with increased precipitation and SST, contributing to an increase in frequency and intensity of tropical storms. Of note, 2009–2010 had an El Niño cycle immediately followed by La Niña 2010–2012. Within this period, 2010 had some of the strongest interannual SST variability, with a strong cold anomaly in the winter that lasted until April, and a warm anomaly starting in May that was strongest from June 2010 to February 2011. From 2014 to 2016, the PR region was exposed to a strong El Niño followed by La Niña conditions from 2016 to 2018 [37], with hurricanes Irma and Maria in 2017 being some of the most devastating natural disasters on record [2]. Within this period, 2016 was another transitional year, with El Niño lasting until May and La Niña starting in July, however in this case, the anomalies of both cycles were weaker than in 2010. Finally, a weaker El Niño was recorded from August 2018 to July 2019, and conditions remained neutral until July 2020 giving way to a multi-year La Niña that lasted until February 2023.

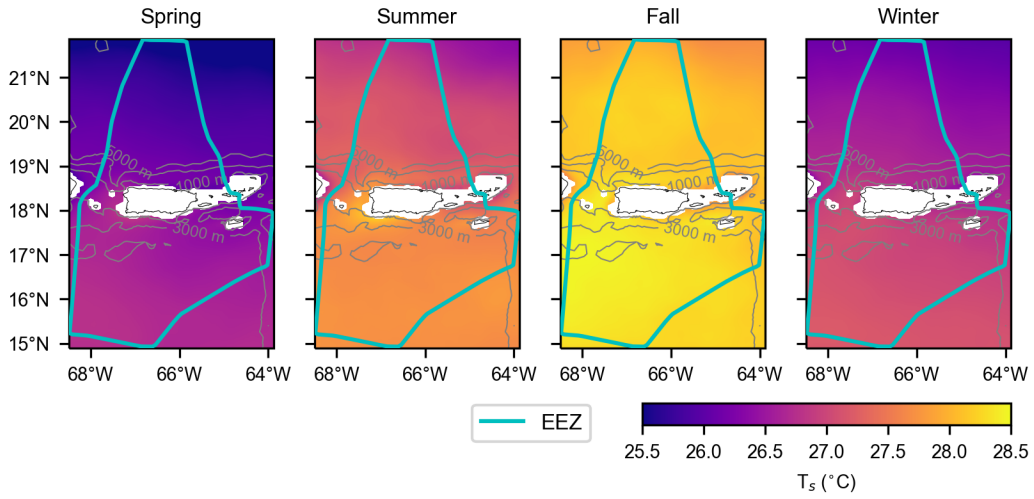

Figure 5: Seasonal distributions of surface temperature, T_s, at a 50 m depth. Regions that are shallower than 50 m are shown in white.

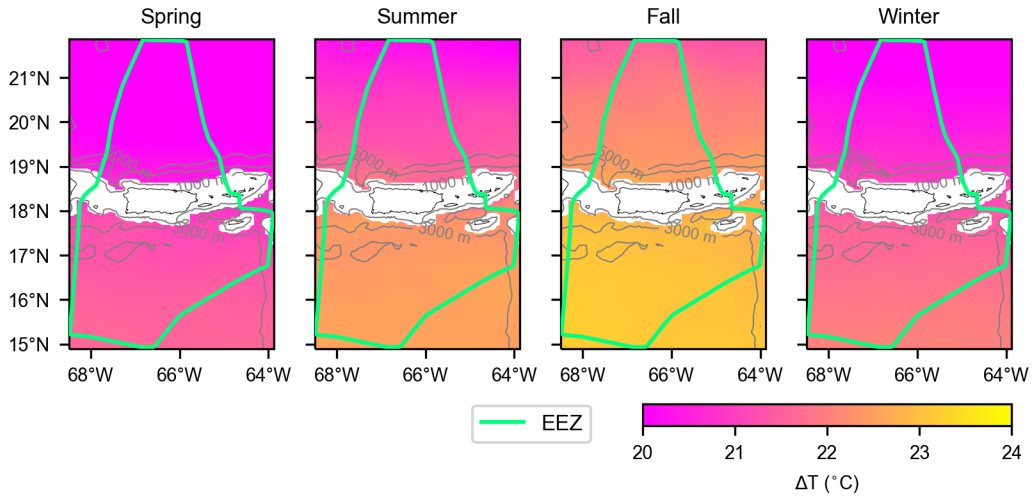

Figure 6: Seasonal distributions of temperature differentials, ΔT, between a warm water depth of 50 m and a sample cold water depth of 1,000 m. Regions that are shallower than 1,000 m are shown in white.

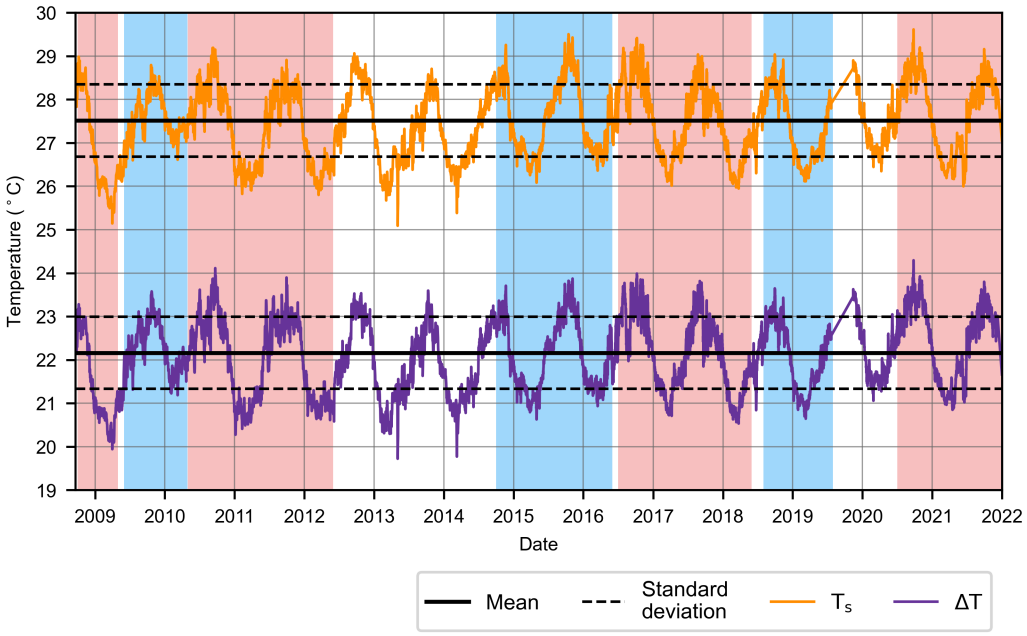

Figure 7: Time series of cluster S1 surface temperature (T_s) at 50 m, and temperature differential (ΔT) at a sample cold water depth of 1,000 m. El Niño periods are shaded in blue and La Niña periods are shaded in red.

3.2. OTEC power production estimates

The theory of heat engine technology suggests that a minimum temperature differential of 20^{o}C is required for OTEC operation [7, 9]. This is because the efficiency of heat engines is a function of ΔT, influencing most aspects of the design including the pipe sizes, heat exchangers, and turbogenerators [34]. This operational limitation is applied to the analysis of OTEC power generation potential by assuming that a plant would not produce any power below the 20^{o}C temperature differential threshold. Seasonal and annual power density maps for OTEC systems in PR and the USVI with a sample cold water depth of 1,000 m are shown in Figures 8 and 9. Regions

that on average do not meet the threshold of a minimum thermal gradient of 20^oC at this depth are masked in white. This includes shallow regions with water depths below 1,000 m, and regions where the threshold would only be met when pumping cold water from deeper elevations. The thermal resource fluctuates seasonally by up to 200 $kW/m^3/s$, with the lowest and greatest energy potentials observed in the spring and in the fall, respectively. In the Caribbean Sea, south of PR, the thermal energy potential is greater than to the north in the Atlantic Ocean by up to 100 $kW/m^3/s$. The resource to the north is also slightly less seasonally consistent than to the south, likely due to the influence of colder winter storms in the Atlantic Ocean which cool the sea surface and in turn reduce ΔT.

The interannual OTEC power variability is directly influenced by the local climate variability and in particular the ENSO anomalies as shown in Figure 7 and Figure 10. The greatest annual OTEC power potential was in 2010, and to a lesser degree in 2016, and 2020, all linked to years that mark the beginning of La Niña conditions in the summer, following either El Niño (2010 and 2016) or neutral winter conditions (2020). This is likely because at the start of La Niña, the deep water temperature remains cooler as the SST begins to increase, therefore increasing the thermal gradient and in turn the OTEC power potential. The mean power density is 2.2% greater during years that transition to La Niña conditions (2010, 2016 and 2020) as compared to the full data records, whereas years that transition to El Niño conditions (2009, 2015 and 2019) are lower on average by 1.3%.

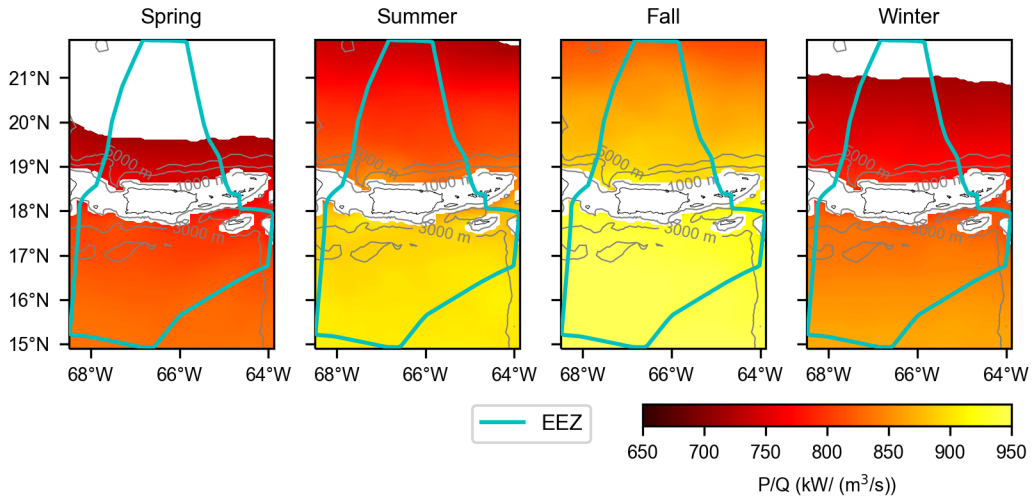

Figure 8: Seasonal variability of OTEC power density per unit of cold water inflow at a sample cold water intake depth of 1 km.

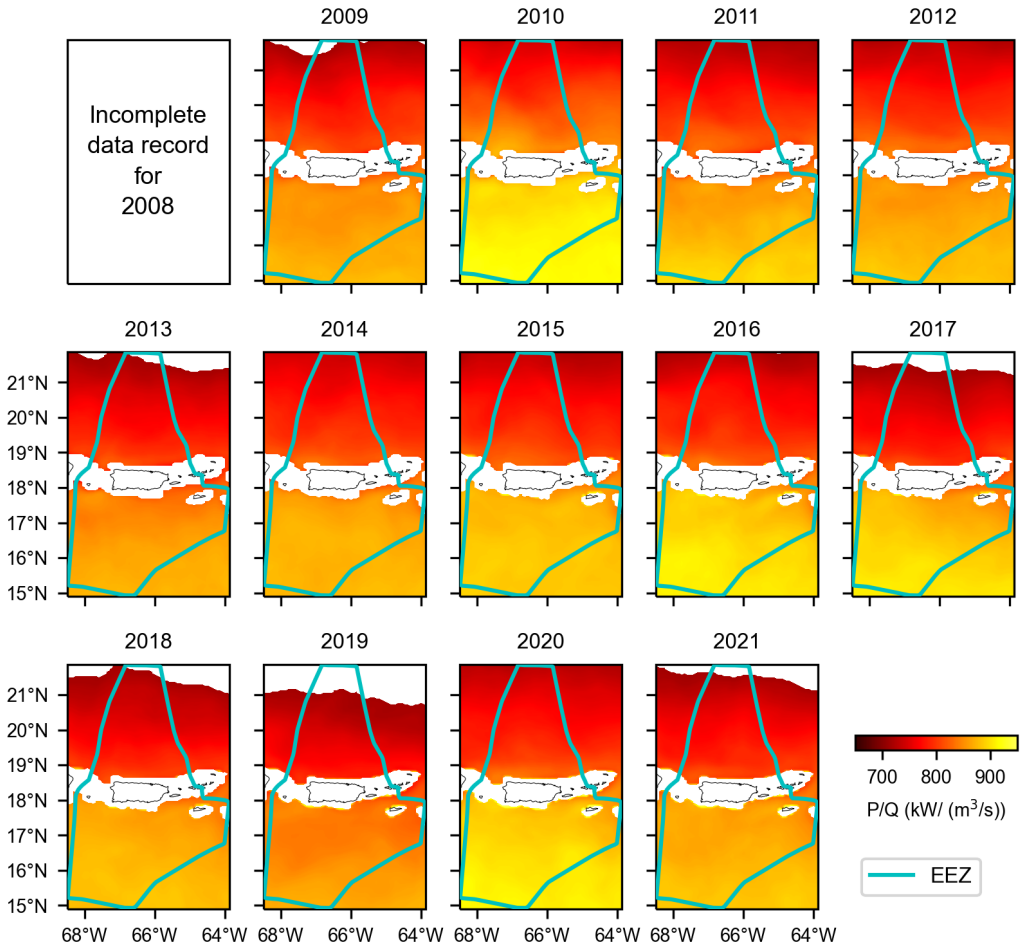

Figure 9: Annual variability of OTEC power density per unit of cold water inflow at a sample cold water intake depth of 1 km.

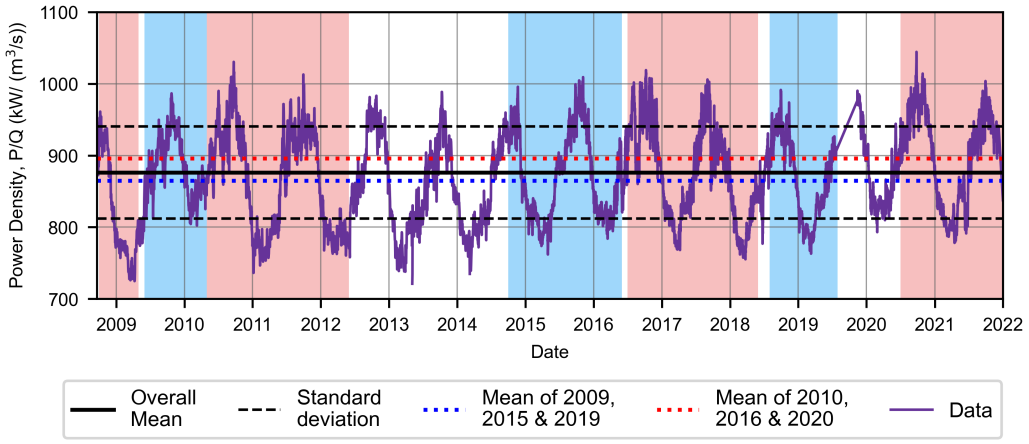

Figure 10: Time series of cluster S1 power density at a sample cold water depth of 1,000 m. El Niño periods are shaded in blue and La Niña periods are shaded in red.

3.3. Cold water intake depth considerations

A limitation of calculating the geospatial OTEC energy potential based on a single isobath for the collection of cold water, is that it prevents optimization of the length of the cold water intake pipe, which in general should be as short as possible to minimize installation and maintenance costs [22]. An alternative approach is to determine the depth at which the minimum temperature gradient criterion is met at each location in the domain. Figure 11.a shows the distribution of depths at which the thermal gradient between the cool deep water and warm surface water is equal to 20^{o}C based on the 14-year data average. Regions masked in white close to shore are too shallow to meet this threshold. Figure 11.b shows areas of interest that will be used for a time series analysis in Section 4. The intra-annual variability in the thermal resource has a direct relation with the depth at which the minimum temperature gradient criterion is met. In the fall as compared to

the spring, the minimum depth from which an OTEC plant could upwell cold water is lower by about 150–225 m in coastal regions (Figure 12). In general, the depth at which the operational threshold is met is lower to the south of PR than to the north.

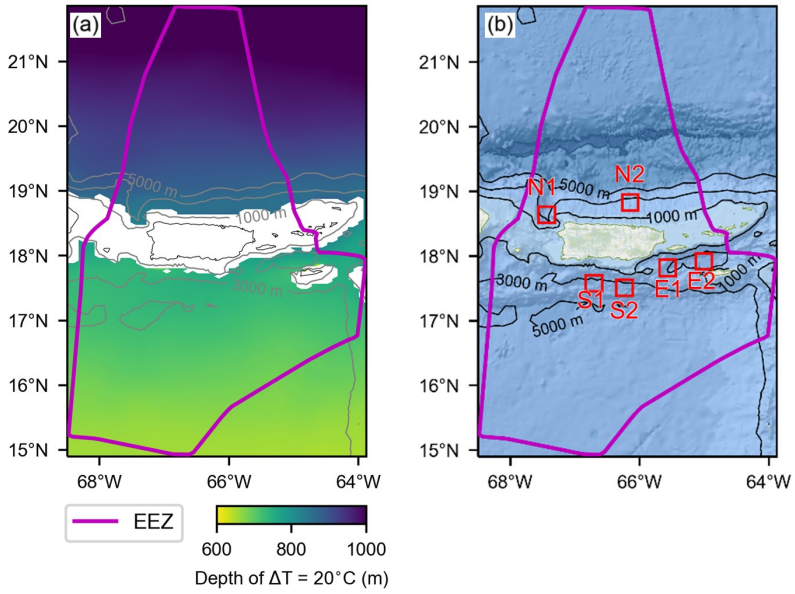

Figure 11: (a) Distribution of depths where the thermal gradient ΔT is equal to 20^oC based on the 14-year annual average. (b) Location of data clusters for time-series analysis.

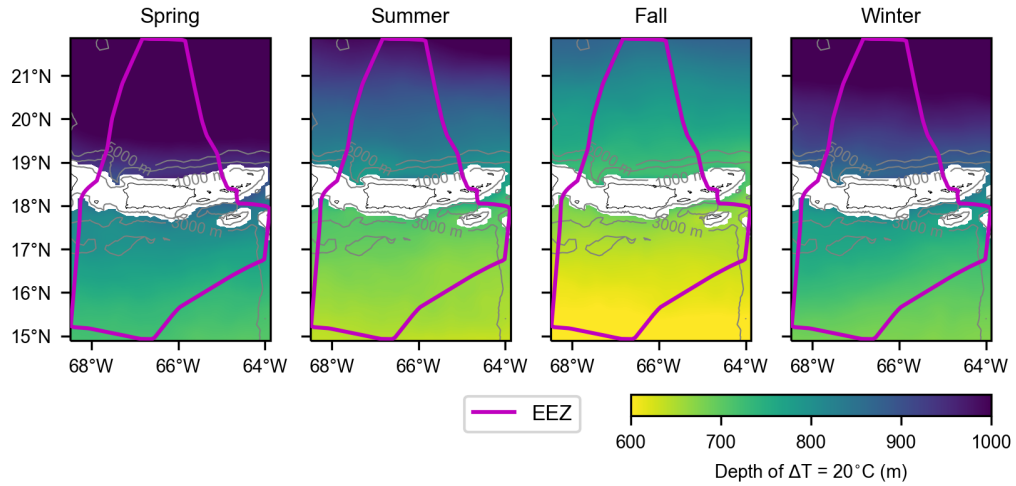

Figure 12: Seasonal distribution of depths where the thermal gradient ΔT is on average equal to 20^oC.

4. Discussion

While a temporally averaged analysis is useful for obtaining an approximate estimate of the power density and identifying the relative geographic potential of OTEC at a given depth, it overrepresents the available power because the averaging calculations include times when the thermal gradients fall below the critical threshold of 20^oC, when a typical OTEC plant would generate no power. For a more complete assessment of the thermal resource, it is important to analyze the temporal and vertical variability of specific point locations of interest.

Six locations, or data clusters, were selected around PR and the USVI for a more in-depth analysis of the OTEC potential (Figure 11.b). Each data cluster represents 9 nodes in the HYCOM computational grid and is located at the shortest viable distance from an existing electrical transmission

line, excluding the nearshore regions that are depth-limited in achieving the minimum operational thermal gradient per Figure 11.a. Information about PR's power plants and major transmission lines was obtained from [38], which provides comprehensive details about the top energy sources (petroleum, natural gas and coal) as well as additional energy sources including solar, wind, hydroelectric and biomass. The selection of sites close to existing transmission lines is intended to offset the high capital costs inherent with installing OTEC plants. OTEC plants located at the northern and southern clusters (N1, N2, S1, and S2) would have the potential to serve the main island which is where the majority of PR's population resides. The highest population density is concentrated on the northern coast (near N2) around the capital city of San Juan [39] and is therefore a region of high power consumption. However, the largest power generating plants are located in the south (near S1 and S2). Cluster E1, and to a lesser degree E2, could supply power for Vieques island, just east of the mainland, which currently imports its power from the mainland. E2 is also used as a benchmark for the OTEC power that could be supplied to the island of St. Croix, USVI. An OTEC plant near St. Croix would likely need to be connected to existing power transmission lines in Christiansted to the noth-norheast of the island [40]. All of these locations were selected as representative case studies; optimization or micro-siting of OTEC infrastructure is not considered at this stage.

Figure 13 shows the exceedance probability of OTEC power density for each data cluster, considering two different cold water intake depths (800 m and 1,000 m) as well as distinguishing between times that the temperature differential is below and above the critical threshold of 20^{o}C (dashed and solid

lines, respectively). Assuming that no power is produced for temperature differentials below the critical threshold, this analysis can be used to estimate the percent time of operation of each plant. For cold water withdrawn at a 1,000 m depth, all OTEC plants would have operated nearly nonstop based on the 14-year HYCOM dataset, typically exceeding a minimum power density of 720–760 kW/m^3/s and reaching a maximum of 1,000–1,025 kW/m^3/s. For cold water withdrawn at a 800 m depth, clusters S1 and S2 have the highest times of operation (83–86%), while cluster N2 has the lowest (58%). At this depth the operational OTEC power density typically exceeds a minimum of 700–720 kW/m^3/s and reaches a maximum of 900–925 kW/m^3/s.

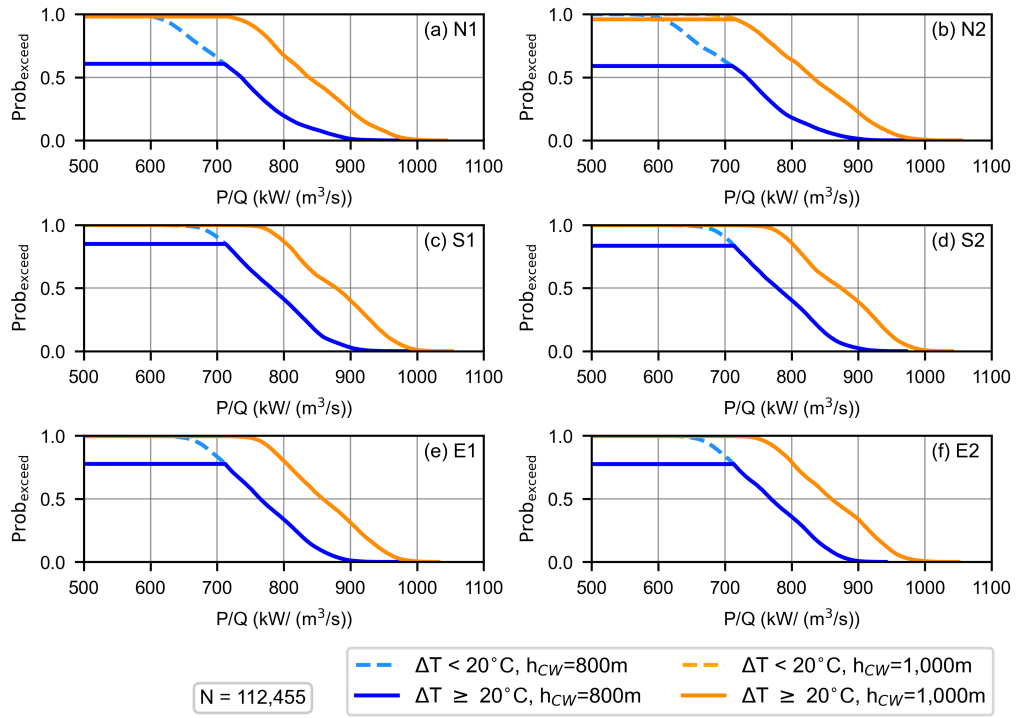

Figure 13: Exceedance probability of OTEC power density at data clusters to the (**a**–**b**) north, (**c**–**d**) south, and (**e**–**f**) east of PR. Number of observations in the dataset: 112,455.

Power production depends on the volumetric flowrate of the upwelled cold water, which is calculated from the product of the upwelling speed (assuming a typical value of 2 m/s[7, 22, 14]) times the area of the intake pipe. Summaries of OTEC power potential for cold water intake pipes of different diameters (2.5 m, 6.5 m and 10 m) and fixed depths of 800 m and 1,000 m are provided in Table 2 and Table 3, respectively. Each of the pipe diameters was chosen to represent a different plant scale. A 2.5 m diameter represents the largest commercially available HDPE underwater pipe and it is suitable for demonstration small-scale plants [22] of under 10 MW. The 6.5 m and 10 m

diameter pipes, were selected to obtain mid-size and full-size plant capacities of about 50 MW and 100 MW, respectively. Consistent with the exceedance probability plots, the highest OTEC potential corresponds to clusters S1 and S2. Time of operation varies more significantly between clusters for the shallower cold water pipe depth (from 58% to 86%) leading to more significant differences in the annual energy production (from 583 to 935 thousand MWh or a 352 thousand MWh difference). For the 1,000 m pipe depth, the maximum difference between clusters in the AEP is 106 thousand MWh.

Figure 14.a shows the monthly electricity production at all clusters using a sample cold water pipe depth of 1,000 m and pipe diameters of 6.5 m and 10 m. At all cluster locations, increasing the pipe diameter from 6.5 m to 10 m results in about a 60 thousand MWh increase in electricity production. The lowest variability between OTEC plant locations is seen in October, which is associated with the largest temperature gradients and therefore the highest times of operation. Conversely, the highest variability between OTEC plant locations is seen in February (by up to 10 thousand MWh), which is associated with the lowest temperature gradients and therefore the lowest times of operation. Figure 14.b shows the monthly electricity use in PR in 2022 by end-use sector obtained from the U.S. Energy Information Administration (EIA) annual electric power report for 2022 [41]. From November to February, the OTEC electricity production potential as well as the historical electrical use are relatively low. After March, the OTEC electricity production potential increases steadily up to a peak in October. While the industrial electricity use is basically constant throughout the year, the residential and commercial demand is highest during the warmer months (June–September)

and is at its lowest in October. On average, a full-scale plant with a 10 m cold water pipe at a 1,000 m depth, would be able to power about 200,000 households or about 17% of all households. Therefore, six of such OTEC plants would be able to power all of the households in PR.

Table 2: Summary of OTEC power potential for cold water intake pipes of variable diameters, D, at a fixed cold water intake depth of 800 m.

Cluster	**Site**	**Time of operation (%)**	**Capacity (MW)**			**AEP (Thousand MWh)**		
			D = 2.5m	**D = 6.5m**	**D = 10m**	**D = 2.5m**	**D = 6.5m**	**D = 10m**
N1	Aguadilla	59.5	4.3	29	69	38	254	602
N2	San Juan	58.1	4.2	28	67	36	246	583
S1	Peñuelas	83.9	6.4	44	103	56	382	903
S2	Salinas	82.7	6.3	43	101	56	375	888
E1	Vieques	75.9	5.7	39	92	50	339	802
E2	Vieques / St. Croix	76.4	5.8	39	92	51	342	809

Table 3: Summary of OTEC power potential for cold water intake pipes of variable diameters, D, at a fixed cold water intake depth of 1,000 m.

Cluster	**Site**	**Time of operation (%)**	**Capacity (MW)**			**AEP (Thousand MWh)**		
			D = 2.5m	**D = 6.5m**	**D = 10m**	**D = 2.5m**	**D = 6.5m**	**D = 10m**
N1	Aguadilla	98.2	8.1	55	130	71	481	1,139
N2	San Juan	95.8	7.8	53	126	69	465	1,100
S1	Peñuelas	100	8.6	58	138	75	510	1,206
S2	Salinas	99.8	8.6	58	137	75	507	1,199
E1	Vieques	99.6	8.4	57	135	74	499	1,181
E2	Vieques / St. Croix	99.7	8.4	57	135	74	500	1,182

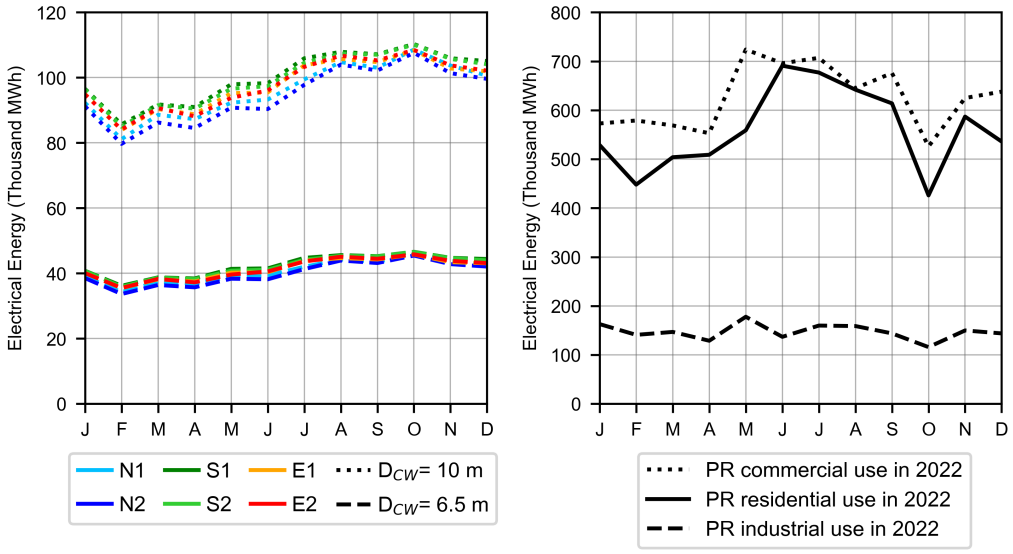

Figure 14: (**a**) Monthly electricity production by OTEC plants using different cold water intake pipes of varied diameters (6.5 m and 10 m) at a sample depth of 1,000 m. (**b**) PR electricity use by end-use sector in 2022.

5. Conclusions

OTEC technology is used to generate power from the vertical thermal gradients in the ocean's water column and is most suitable for tropical regions. The thermal resource potential around PR and the USVI was characterized based on a 14-year dataset of modeled ocean temperature obtained from HYCOM. The assessment shows the effects that geographical, seasonal, and interannual variability have on OTEC power production. In general, the thermal gradients near PR on the side of the Caribbean Sea are greater than on the side of the Atlantic Ocean if considering plants with cold water intake pipes installed at equal depths; close to the mainland of PR, the difference is about 1^{o}C. The greatest seasonal thermal gradients, and in turn great-

est OTEC power density, were observed in the fall (about 950 kW/m^3/s), particularly in October, whereas the lowest were observed in the winter (about 750 kW/m^3/s), particularly in February. The interannual variability is closely linked to ENSO cylces, with the lower power potential observed during El Niño conditions and the higher power potential during La Niña conditions. In particular years in which El Niño or neutral conditions transition to La Niña conditions, are linked to the highest OTEC power densities.

Optimal depths for operation were computed taking advantage of the fine vertical resolution of the model based dataset (33 to 40 vertical layers). The analysis considers the availability of a minimum thermal gradient of 20^{o}C between the warm sea surface and cool deep water needed for OTEC operation. This approach helped exclude regions close to shore that are depth-limited and could never meet this threshold. In combination with the power density distributions, these results were also used to select six areas of opportunity based on their resource potential, shortest distance to shore (which would reduce the costs of transferring energy to shore), and proximity to existing electrical distribution lines in PR, including one sites that could also benefit the nearby USVI island of St. Croix. The greatest OTEC power potential is associated with locations in the Caribbean Sea, particularly to the south of PR. At these sites the estimated OTEC plant capacity with a 10 m diameter and 1,000 m deep pipe would be about 137 MW, each producing 1.2 TWh of annual power, the amount required to power 219,000 households or 17% of the total residential electricity demand based on 2022 usage data in PR.

The criteria prioritized for site selection in this study was based on tech-

noeconomic factors: minimal cold water intake depths to reduce piping and pumping lengths, shortest distance to shore to minimize electric cable lengths, and proximity to existing transmission lines to reduce expected capital costs. While environmental factors and logistical considerations (e.g., fishing zones) are outside the scope of this study, these are important constraints for the eventual installation of any OTEC plant and would be a natural next step to consider in a future study.

References

[1] Electric Power Authority (PREPA), Puerto Rico Energy Public Policy Act No. 17-2019 (2019).
URL https://bvirtualogp.pr.gov/ogp/Bvirtual/leyesreferencia/PDF/2-ingles/17-2019.pdf

[2] M. Baggu, R. Burton, N. Blair, M. Sengupta, T. Harris, C. Barrows, H. Sky, V. Gevorgian, J. Keen, E. Smith, M. Campton, S. Jena, J. Yang, T. Williams, P. Das, J. Elsworth, P. Joshi, C. Weiner, J. Morris, J. McKinsey, S. C. Dhulipala, S. Molnar, W. Yan, P. Sharma, W. Wang, A. Latif, D. Thom, S. Dalvi, I. Baring-Gould, M. Lave, A. Wachtel, C. B. Jones, E. Moog, A. Mammoli, R. Garrett, T. Haines, W. Vining, C. Newlun, O. Hart, M. Elizondo, X. Fan, P. Maloney, A. Bharati, B. Vyakaranam, V. Chalishazar, P. Royer, F. Bereta dos Reis, X. M. Li, K. Mahapatra, J. Dagle, X. Ke, M. Zhao, O. Vasios, T. Franklin, M. Abdelmalak, K. Guddanti, S. Acharya, M. Cruz, P. Etingov, C. Qin, J. C. Bedoya, T. Nguyen, S. Bhadra, A. Tbaileh, L. Ward, V. Sinnott, P. Mendez-Curbelo, P. Cappers, J. Deason, M. Pigman, L. P.

Lewis, J. T. Murphy, T. Kobayashi-Carvalhaes, M. Bennett, Y. Liu, H. Cutler, M. Shields, H. Jeon, M. Chait, Puerto Rico Grid Resilience and Transitions to 100% Renewable Energy Study (PR100): Final Report, Tech. Rep. NREL/TP-6A20-88384, National Renewable Energy Laboratory (NREL), Golden, CO (United States) (Mar. 2024). doi:10.2172/2335361.

[3] LUMA, Generation Resource Adequacy Analysis, Tech. rep., Puerto Rico Energy Bureau (PREB) (Aug. 2022).
URL https://energia.pr.gov/wp-content/uploads/sites/7/2022/09/Motion-to-Submit-Lumas-Resource-Adequacy-Study-NEPR-MI-2022-0002.pdf

[4] U.S. EIA, EIA Puerto Rico Profile, accessed 8 April 2024 (Feb. 2024).
URL https://www.eia.gov/state/print.php?sid=RQ

[5] M. B. Ascari, H. P. Hanson, L. Rauchenstein, J. Van Zwieten, D. Bharathan, D. Heimiller, N. Langle, G. N. Scott, J. Potemra, N. J. Nagurny, E. Jansen, Ocean Thermal Extractable Energy Visualization, Tech. Rep. DE-EE0002664, Lockheed Martin Mission Systems and Sensors (Oct. 2012). doi:10.2172/1055457.

[6] C. Wu, A performance bound for real OTEC heat engines, Ocean Engineering 14 (4) (1987) 349–354. doi:10.1016/0029-8018(87)90032-1.

[7] L. A. Vega, Ocean Thermal Energy Conversion Primer, Marine Technology Society Journal 36 (4) (2002) 25–35. doi:10.4031/002533202787908626.

[8] Y. Ikegami, T. Yasunaga, T. Morisaki, Ocean Thermal Energy Conversion Using Double-Stage Rankine Cycle, Journal of Marine Science and Engineering 6 (1) (2018) 21, number: 1 Publisher: Multidisciplinary Digital Publishing Institute. doi:10.3390/jmse6010021.

[9] L. A. Vega, Ocean Thermal Energy Conversion, Springer, New York, NY, 2012, in R. A. Meyers (eds) Encyclopedia of Sustainability Science and Technology, pp. 7296–7328. doi:10.1007/978-1-4419-0851-3_695.

[10] S. M. Abbas, H. D. S. Alhassany, D. Vera, F. Jurado, Review of enhancement for ocean thermal energy conversion system, Journal of Ocean Engineering and Science 8 (5) (2023) 533–545. doi:10.1016/j.joes.2022.03.008.

[11] G. C. Nihous, A Preliminary Assessment of Ocean Thermal Energy Conversion Resources, Journal of Energy Resources Technology 129 (1) (2007) 10–17. doi:10.1115/1.2424965.

[12] K. Rajagopalan, G. C. Nihous, Estimates of global Ocean Thermal Energy Conversion (OTEC) resources using an ocean general circulation model, Renewable Energy 50 (2013) 532–540. doi:10.1016/j.renene.2012.07.014.

[13] D. E. Cavrot, Economics of Ocean Thermal Energy Conversion (OTEC), Renewable Energy 3 (8) (1993) 891–896. doi:10.1016/0960-1481(93)90047-K.

[14] J. Herrera, S. Sierra, H. Hernández-Hamón, N. Ardila, A. Franco-Herrera, A. Ibeas, Economic Viability Analysis for an OTEC Power Plant at San Andrés Island, Journal of Marine Science and Engineering 10 (6) (2022) 713, number: 6 Publisher: Multidisciplinary Digital Publishing Institute. doi:10.3390/jmse10060713.

[15] W. L. Owens, L. C. Trimble, Mini-OTEC Operational Results, Journal of Solar Energy Engineering 103 (3) (1981) 233–240. doi:10.1115/1.3266245.

[16] T. Mitsui, F. Ito, Y. Seya, Y. Nakamoto, Outline Of The 100 kw Otec Pilot Plant In The Republic Of Naure, IEEE Transactions on Power Apparatus and Systems PAS-102 (9) (1983) 3167–3171, conference Name: IEEE Transactions on Power Apparatus and Systems. doi:10.1109/TPAS.1983.318124.

[17] D. Vera, A. Baccioli, F. Jurado, U. Desideri, Modeling and optimization of an ocean thermal energy conversion system for remote islands electrification, Renewable Energy 162 (2020) 1399–1414. doi:10.1016/j.renene.2020.07.074.

[18] Y. Ohki, News from Japan: Ocean thermal energy conversion development center in Okinawa, IEEE Electrical Insulation Magazine 36 (3) (2020) 47–50, conference Name: IEEE Electrical Insulation Magazine. doi:10.1109/MEI.2020.9063563.
URL https://ieeexplore.ieee.org/document/9063563

[19] M. G. Brown, White Paper on Ocean Thermal Energy Conversion

(OTEC), Tech. rep., Ocean Energy Systems (OES) (Oct. 2021).
URL https://www.ocean-energy-systems.org/publications/oes-position-papers/document/white-paper-on-otec/

[20] M. G. Petterson, H. J. Kim, Can Ocean Thermal Energy Conversion and Seawater Utilisation Assist Small Island Developing States? A Case Study of Kiribati, Pacific Islands Region, in: A. S. Kim, H.-J. Kim (Eds.), Ocean Thermal Energy Conversion (OTEC), IntechOpen, Rijeka, 2020, Ch. 1. doi:10.5772/intechopen.91945.
URL https://doi.org/10.5772/intechopen.91945

[21] R. Fujita, A. C. Markham, J. E. Diaz Diaz, J. Rosa Martinez Garcia, C. Scarborough, P. Greenfield, P. Black, S. E. Aguilera, Revisiting ocean thermal energy conversion, Marine Policy 36 (2) (2012) 463–465. doi:10.1016/j.marpol.2011.05.008.

[22] C. Bernardoni, M. Binotti, A. Giostri, Techno-economic analysis of closed OTEC cycles for power generation, Renewable Energy 132 (2019) 1018–1033. doi:10.1016/j.renene.2018.08.007.

[23] G. Heydt, An assessment of ocean thermal energy conversion as an advanced electric generation methodology, Proceedings of the IEEE 81 (3) (1993) 409–418, conference Name: Proceedings of the IEEE. doi:10.1109/5.241487.

[24] G. C. Nihous, An estimate of Atlantic Ocean thermal energy conversion (OTEC) resources, Ocean Engineering 34 (17) (2007) 2210–2221. doi:10.1016/j.oceaneng.2007.06.004.

[25] Y. Jia, G. C. Nihous, K. Rajagopalan, An Evaluation of the Large-Scale Implementation of Ocean Thermal Energy Conversion (OTEC) Using an Ocean General Circulation Model with Low-Complexity Atmospheric Feedback Effects, Journal of Marine Science and Engineering 6 (1) (2018) 12, number: 1 Publisher: Multidisciplinary Digital Publishing Institute. doi:10.3390/jmse6010012.

[26] T. Du, Z. Jing, L. Wu, H. Wang, Z. Chen, X. Ma, B. Gan, H. Yang, Growth of ocean thermal energy conversion resources under greenhouse warming regulated by oceanic eddies, Nature Communications 13 (1) (2022) 7249, publisher: Nature Publishing Group. doi:10.1038/s41467-022-34835-z.

[27] J. H. VanZwieten, L. T. Rauchenstein, H. P. Hanson, M. R. Dhanak, Assessment of HYCOM as a tool for estimating Florida's OTEC potential, in: OCEANS'11 MTS/IEEE KONA, Waikoloa, HI, USA, 2011, pp. 1–8. doi:10.23919/OCEANS.2011.6107134.

[28] J. H. VanZwieten, L. T. Rauchenstein, L. Lee, An assessment of Florida's ocean thermal energy conversion (OTEC) resource, Renewable and Sustainable Energy Reviews 75 (2017) 683–691. doi:10.1016/j.rser.2016.11.043.

[29] A. Devis-Morales, R. A. Montoya-Sánchez, A. F. Osorio, L. J. Otero-Díaz, Ocean thermal energy resources in Colombia, Renewable Energy 66 (2014) 759–769. doi:10.1016/j.renene.2014.01.010.

[30] J. R. S. Doorga, O. Gooroochurn, B. A. Motah, V. Ramchandur,

S. Sunassee, A novel modelling approach to the identification of optimum sites for the placement of ocean thermal energy conversion (OTEC) power plant: application to the tropical island climate of Mauritius, International Journal of Energy and Environmental Engineering 9 (4) (2018) 363–382. doi:10.1007/s40095-018-0278-4.

[31] E. P. Garduño-Ruiz, R. Silva, Y. Rodríguez-Cueto, A. García-Huante, J. Olmedo-González, M. L. Martínez, A. Wojtarowski, R. Martell-Dubois, S. Cerdeira-Estrada, Criteria for Optimal Site Selection for Ocean Thermal Energy Conversion (OTEC) Plants in Mexico, Energies 14 (8) (2021) 2121, number: 8 Publisher: Multidisciplinary Digital Publishing Institute. doi:10.3390/en14082121.

[32] J. Marina, F. Perez, Proposed OTEC Punta Tuna Pilot Plant, in: AIWA Terrestrial Energy Systems Conference 2, Vol. 81-2565, Colorado Springs, CO, USA, 1981.
URL https://www.osti.gov/biblio/5461444

[33] B. W. Dambly, A 40 MWe floating OTEC plant at Punta Tuna, Puerto Rico, in: AIWA Terrestrial Energy Systems Conference 2, Vol. 81-2564, Colorado Springs, CO, USA, 1981.
URL https://www.osti.gov/biblio/5391939

[34] National Research Council, An Evaluation of the U.S. Department of Energy's Marine and Hydrokinetic Resource Assessments, The National Academies Press, Washington, D.C., 2013. doi:10.17226/18278.
URL http://www.nap.edu/catalog/18278

[35] L. Kilcher, M. Fogarty, M. Lawson, Marine Energy in the United States: An overview of opportunities, Tech. Rep. NREL/TP-5700-78773, National Renewable Energy Laboratory (2021). doi:10.2172/1766861.

[36] HYCOM Consortium for Data Assimilative Modeling, HYCOM Sata Server, accessed 12 December 2022.
URL https://www.hycom.org/dataserver

[37] R. Barrera, V. Acevedo, M. Amador, M. Marzan, L. E. Adams, G. Paz-Bailey, El Niño Southern Oscillation (ENSO) effects on local weather, arboviral diseases, and dynamics of managed and unmanaged populations of Aedes aegypti (Diptera: Culicidae) in Puerto Rico, Journal of medical entomology 60 (4) (2023) 796–807. doi:10.1093/jme/tjad053.

[38] M. Sotolongo, L. Kuhl, S. H. Baker, Using environmental justice to inform disaster recovery: Vulnerability and electricity restoration in Puerto Rico, Environmental Science & Policy 122 (2021) 59–71. doi:10.1016/j.envsci.2021.04.004.

[39] U.S. Census Bureau, Population Density in Puerto Rico Counties: 2020 (Aug. 2021).
URL https://www.census.gov/library/visualizations/interactive/2020-population-and-housing-state-data.html

[40] C. E. Clark, R. J. Campbell, D. A. Austin, Potential Options for Electric Power Resiliency in the U.S. Virgin Islands, Tech. Rep. R45105, Congressional Research Service (Feb. 2018).
URL https://sgp.fas.org/crs/row/R45105.pdf

[41] U.S. EIA, Electric Power Annual 2022, Tech. rep., U.S. Energy Information Administration (Oct. 2023).
URL https://www.eia.gov/electricity/annual/pdf/epa.pdf